

COMPARISON OF RECOMBINATION ACTIVITY OF GRAIN BOUNDARIES IN VARIOUS MULTICRYSTALLINE SILICON MATERIALS

H. C. Sio¹, S. P. Phang¹, H. T. Nguyen¹, D. Yan¹, T. Trupke² and D. Macdonald¹

¹Research School of Engineering, The Australian National University (ANU), Canberra ACT 0200, Australia.

²School of Photovoltaic and Renewable Energy Engineering, The University of New South Wales (UNSW), Sydney NSW 2052, Australia

ABSTRACT: We compare the recombination properties of grain boundaries in conventionally-solidified p-type, n-type and ‘high performance’ p-type multicrystalline silicon wafers in terms of their surface recombination velocities, and evaluate their response to phosphorus gettering and hydrogenation. Overall, grain boundaries in the conventional p-type samples were found to be more recombination active than those in the high performance p-type and conventional n-type samples. As-grown grain boundaries in high performance multicrystalline silicon were not recombination active and only became active after thermal processes. In contrast, grain boundaries in the n-type samples were already recombination active in the as-grown state, but show a dramatic reduction in their recombination strength after gettering and hydrogenation. Distinct sub-bandgap photoluminescence spectra were detected from grain boundaries that are already active before gettering, and also those activated by gettering, suggesting different origins for their recombination activities. Moreover, the detrimental influence of grain boundaries on solar cell devices is discussed with the aid of numerical simulations.

Keywords: carrier lifetime, grain boundaries, multicrystalline silicon, photoluminescence imaging, recombination

1 INTRODUCTION

Grain boundaries (GBs) are one type of crystal defect which significantly affects the efficiency of multicrystalline silicon (mc-Si) solar cells. The electrical properties of GBs depend on the geometry of the GBs, the contamination levels in the materials, and their interactions [1-4]. It has also been shown that their properties change after phosphorous gettering [4-8] and hydrogenation [4, 8-11]. Although GBs have been studied extensively in the literature, the underlying mechanisms of GB behaviour are still not fully understood. One of the challenges is the lack of a quantitative method that is suitable to be applied on a large number of GBs, to evaluate their recombination properties for a statistically relevant analysis. In our previous work [12], we proposed a method to quantify the recombination strength of a GBs in terms of the effective surface recombination velocity (S_{eff}), based on photoluminescence (PL) imaging and 2D modelling of the emitted PL profile. In this work, we apply this method to compare the recombination properties of a relatively large number of GBs from three different types of mc-Si materials, namely conventionally-solidified p-type and n-type mc-Si wafers, and also the recently developed ‘high performance’ p-type mc-Si wafers, and investigate their response to phosphorus gettering and hydrogenation. In addition to band-to-band PL imaging, we also study sub-bandgap PL emitted from several selected GBs by applying a micron-scale PL spectroscopy technique at low temperature.

2 EXPERIMENTAL METHODS

2.1 Sample Preparation

Wafers used in this work were cut from three commercially grown directionally-solidified mc-Si ingots, that is, a conventional p-type boron doped ingot, a conventional n-type phosphorous doped ingot, and a high performance p-type boron doped ingot. The conventional n-type and high performance p-type mc-Si wafers were

around 180 μm and 200 μm thick respectively and have a similar background doping of around $1.2 \times 10^{16} \text{ cm}^{-3}$. The conventional p-type mc-Si wafers were around 330 μm thick with a background doping of $1.5 \times 10^{16} \text{ cm}^{-3}$. Wafers with similar background doping were selected in this work to avoid its potential impact on carrier lifetime, thus allowing direct comparisons between the materials.

Phosphorous gettering was performed through subjecting the wafers to a 30 min POCl_3 diffusion at 880°C, followed by an extended annealing in an N_2 ambient for more than 12 hours at 600°C in the same diffusion furnace, resulting in sheet resistance values of around $20 \Omega/\square$ measured using a 4-point probe. Hydrogenation is achieved by coating the samples with silicon nitride films and firing in a rapid thermal processing (RTP) furnace (Unitemp UTP-1100) for 3 min at 700°C in N_2 ambient. The sample preparation procedures are described in detail in Ref. [13].

For PL measurements, the wafers were divided into two groups. Half of the sister wafers received silicon nitride films on both surfaces for passivation, while the other half of the wafers received silicon nitride films on the front surfaces and thin metallic aluminium films (approximately 10 nm) on the rear surfaces using thermal evaporation, to achieve instantaneous rear surface recombination conditions. The double-side passivated wafers were used to evaluate the bulk lifetime of the intra-grain regions required for the modelling, while the single-side passivated wafers were used to investigate GB behaviour, using techniques described in more detail in Ref. [12]. The deposited silicon nitride films in this work were around 85 nm thick and were deposited with a Roth & Rau plasma enhanced chemical vapour deposition (PECVD) system with deposition temperatures between 250°C and 300°C.

2.2 Characterisation methods

PL images used in this work have a pixel size of 22 μm and were captured with a BT Imaging LIS-R1 tool, in which an 808 nm laser is used for carrier excitation. A

short pass filter with a cut off wavelength of 1050 nm is fitted in the imaging lens to reduce the impact of lateral light scattering both within the sample itself and within the camera's CCD chip. Image deconvolution using an experimentally determined point-spread function (PSF) was applied to the PL images to further reduce the impact of image blurring caused by cross-talk in the CCD chip [14].

The recombination activity of a GB is evaluated in terms of its surface recombination velocity (S_{GB}), determined by fitting the simulated PL profile across the GB, modelled using a finite difference method based on the continuity equation, to an experimental PL profile extracted from a PL image. The details of the method are described in Ref. [12]. The surface recombination velocity (S_{GB}) represents the intrinsic recombination properties of a GB in absolute terms, and does not depend on other parameters such as the lifetime of the intra-grain regions. This allows a direct comparison of GB properties in different materials, before and after various processes.

Micro-photoluminescence spectroscopy was performed with a Horiba Jobin-Yvon T6400 micro-Raman spectrometer. The excitation source is a 532 nm laser with an estimated power of 10mW and a spot size of 2-3 microns. The emission is detected by a liquid nitrogen cooled InGaAs detector.

3 RESULTS

3.1 The Influence of phosphorous gettering and hydrogenation

Fig. 1(a) shows the average lifetimes of the intra-grain regions in the conventional p-type, n-type and high performance p-type mc-Si wafers at approximately 0.1 sun conditions, which corresponds to an injection level close to maximum power in a working solar cell [15]. It can be observed that the intra-grain lifetimes of the n-type samples can reach 1 ms or above and are considerably higher than the other two p-type materials studied here. This is likely to be due to the higher immunity of metal contamination in n-type materials compared to p-type materials [16]. Interestingly, hydrogenation is more effective in n-type materials than p-type materials, being able to further improve the intra-grain lifetime of gettered n-type samples substantially. It is also noted that, although the as-grown intra-grain lifetime of conventional p-type samples is much lower than the high performance p-type samples, their difference largely reduces after gettering and hydrogenation, suggesting that gettering and hydrogenation are very effective in improving the lifetimes of samples with higher levels of impurities.

Fig. 1(b) compares the S_{GB} of GBs from the three groups of samples before and after gettering and hydrogenation. GBs tend to become more recombination active after gettering. Hydrogenation is able to deactivate most of the GBs in n-type samples, while only offset part of the increase in S_{GB} induced by gettering in p-type samples. This echoes the observations above, suggesting that hydrogenation is more effective on n-type mc-Si than p-type mc-Si. The observed behaviour could potentially be related to the charge state of hydrogen. Most of the monatomic hydrogen is positively charged during the high temperature process [17], hence they might be more attractive to negatively charged impurities which are detrimental in n-type materials due to columbic

attraction, improving the effectiveness of hydrogenation.

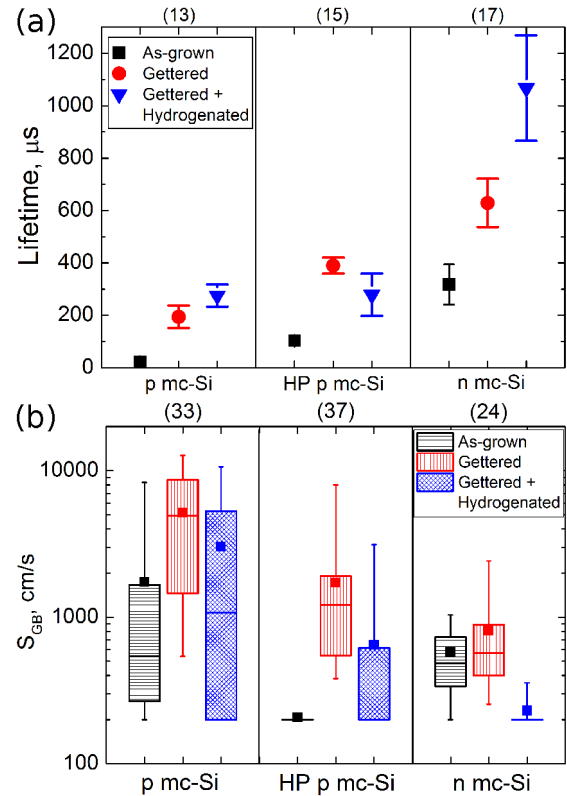


Figure 1: (a) Average τ_{bulk} of several intra-grain regions from conventional p-type (p mc-Si), n-type (n mc-Si) and high performance p-type (HP p mc-Si) mc-Si wafers before and after gettering and hydrogenation. The lifetime values were measured at an injection level equivalent to approximately 0.1 suns. The error bars denote one standard deviation of the data. (b) S_{GB} of various GBs from p mc-Si, n mc-Si and HP mc-Si wafers before and after gettering and hydrogenation. The median values, as well as 25 and 75 percentiles are marked by horizontal bars, the means by squares. The value of 200 cm/s is the lower detection limit of the PL imaging based measurement technique used. The total number of sampled intra-grain regions and GBs are shown above the y-axis.

Overall, as-grown GBs in high performance p-type samples tend not to be recombination active and they become more active after both gettering and hydrogenation. On the other hand, GBs in n-type samples show a completely opposite response. They are already recombination active in the as-grown state, but show a dramatic reduction in their recombination strength after gettering and hydrogenation, with their S_{GB} values dropping below the detection limit of our method. A more detailed analysis, including the response of individual GBs to each specific thermal process, is presented in Ref. [18].

Comparing the two p-type materials, it can be seen that the median S_{GB} value of GBs from conventional p-type samples are considerably higher than the high performance p-type samples. The lower recombination activities of GBs in high performance mc-Si could contribute to the improvement in its cell performance in comparison with conventional p-type mc-Si solar cells, considering that there is little variation in their lifetimes

in the intra-grain region, as described above. This could also explain why the cell efficiency of high performance mc-Si solar cells does not suffer from a higher GB density as a result of smaller grain size in the material.

3.2 Sub-bandgap photoluminescence

In addition to band-to-band PL imaging, micro-PL spectroscopy technique was also applied to measure sub-bandgap PL emitted from several selected GBs in the conventional p-type mc-Si wafers at low temperature (79K), using it as an additional tool to analyse GBs. It is found that distinct sub-bandgap PL spectra were detected from GBs that are already active in the as-grown state and gettering-activated GBs. An example is shown in Fig. 2. GB1 is a $\Sigma 27$ GB, while GB2 is a RA GB with misorientation angle of 33° along the axis [342]. GB2 is not recombination active in the as-grown state, but becomes very active after gettering, while GB1 is active even before gettering. Sub-bandgap PL around 1400 nm is only observed on GB2 after gettering, indicating the possibilities of different origins for the recombination activities in intrinsic active GBs and gettering activated GBs.

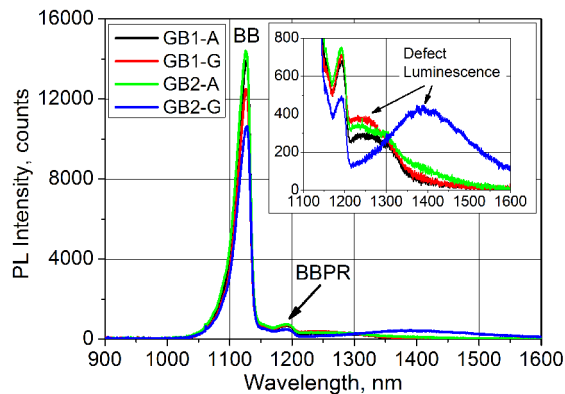


Figure 2: PL spectra of two selected GBs from the conventional p-type mc-Si wafer. A and G denote as-grown and gettered GBs respectively. BB and BBPR denote band-band line and the first phonon replica of the band-band line respectively.

The observed sub-bandgap PL could be related to the well-known dislocation luminescence or D-lines detected from dislocations [19-21]. Tajima *et al.* [21] studied D-lines emitted from dislocation networks or so-called small angle GBs in mc-Si materials and attributed the origin of D1/D2 lines (detected at 1530 and 1410 nm) to secondary defects or impurities trapped by the strain field around the dislocations, and D3/D4 lines (detected at 1330 and 1240 nm) to the intrinsic nature of dislocations. The observed sub-bandgap PL at around 1400 nm from GB2 could be due to the certain types of impurities such as interstitial impurities or small metal precipitates that formed around the GB after gettering. These impurities could be responsible for the dramatic increase in its S_{GB} value. Further studies are needed to identify the root cause for the observed sub-bandgap PL. Nevertheless, the work presented here highlights the possibility of using sub-bandgap PL to detect or identify certain impurities at GBs.

3.3 Activation of GBs in high performance mc-Si during thermal annealing and phosphorous gettering

One of the features observed in this work is that GBs in high performance mc-Si are not recombination active, or only slightly active, before any thermal processes, but become active after gettering and hydrogenation. This could be due to the high temperature applied during the process, or the rapid quenching afterward, that causes a redistribution of impurities near the GBs [13, 22, 23]. In order to clarify the cause of this behaviour, an annealing experiment is performed. Fig. 3 shows PL images of a set of high performance mc-Si wafers that were annealing at various temperatures for 30 minutes in an N_2 ambient. Samples in Fig. 3(b) and (c) were air cooled to room temperature after the anneal, whereas the sample in Fig. 3(d) was slow cooled from 700°C to 400°C with a cooling rate of around $10^\circ C - 15^\circ C$ per 15 minutes and air cooled to room temperature afterward. Being limited by the equipment used, slow cooling from 700°C to room temperature could not be performed. The variation in the PL intensity among different grains in Fig. 3(a) and (d) is due to an orientation dependent surface passivation effect (native oxide for (a) and thermally grown silicon oxide for (b)), as discussed in Ref. [24, 25]. Note that the samples in these PL images are unpassivated, and hence the images are only valid for qualitative comparisons.

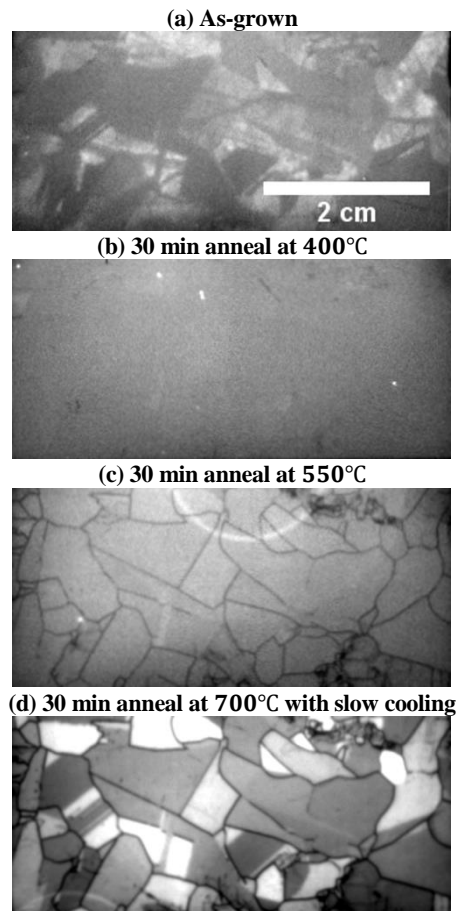


Figure 3: PL images of unpassivated high performance p-type mc-Si wafers before and after thermal annealing. The contrast in each image was adjusted using 50% and 150% of the average PL intensity as the minimum and maximum thresholds. The bright ring appearing in (c) is the inductive coil equipped in the PL imager for the QSSPC lifetime measurement (not used here).

From Fig. 3, it can be seen that GBs in the studied high performance mc-Si are quite stable below 400°C. The activation of GBs occurs between 400°C and 550°C. Even with a slow cooling rate, the activation cannot be avoided, as shown in Fig. 3(d). This indicates that rather than the quenching rate, the anneal temperature is more likely to be the key parameter affecting the recombination properties of GBs in the studied high performance mc-Si ingot.

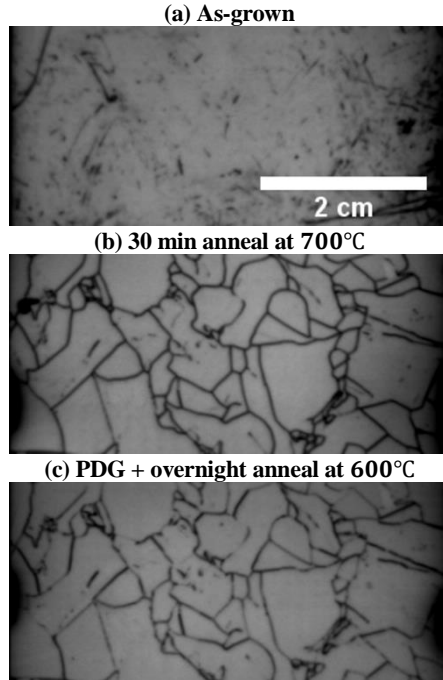


Figure 4: PL images of single-side passivated high performance p-type mc-Si wafers before and after thermal annealing and phosphorous diffusion gettering (PDG). Phosphorus gettering was performed through a 30 minute POCl_3 diffusion at 880°C followed by an overnight anneal. The phosphorous diffused layers were removed before passivation. Both samples in (b) and (c) were air cooled to room temperature after the processes. The contrast in each image was adjusted using 50% and 150% of the PL intensity of an intra-grain region in the image as the minimum and maximum thresholds.

Here, we also compare the effect of thermal annealing to phosphorus gettering. Fig. 4 shows PL images of another set of high performance mc-Si samples before and after thermal annealing and phosphorous gettering. Note that in contrast to those in Fig. 3, single-side passivated samples were used to allow a more direct comparison of the recombination activities of GBs, as explained in detail in Ref. [12]. As shown in Fig. 4, GBs in the wafers were activated by either thermal annealing or gettering. Comparing Fig. 4(b) and (c), it seems that GBs after thermal annealing are more recombination active than those after gettering. This might suggest that a portion of the metal impurities around GBs could in fact be gettering by the phosphorus diffused layers, though the benefit of this effect is overshadowed by the redistribution of metal impurities around the GB as a result of the high temperature used in the process, leading to an overall increase in their recombination behaviour.

3.4 Detrimental influence of GBs on devices

It should be noted that the overall detrimental influence of a GB depends not only on the intrinsic recombination properties of the GB, but also on other conditions such as the surface conditions, the intra-grain lifetime and the operating conditions. Fig. 5 shows the PL intensity profile across a GB with S_{GB} of 1000 cm/s in three different samples: an ideal sample without any surface recombination, a passivated sample and a passivated diffused sample. The total reduction in the PL intensity represents the effective influence of a GB on the neighbouring regions. As illustrated in Fig. 5, surface recombination reduces the overall impact of GBs as it acts as another competing recombination channel for carriers. By contrast, heavily doped layers at the surface provide additional paths for lateral carrier transport, hence further extending the region of influence of GBs [13].

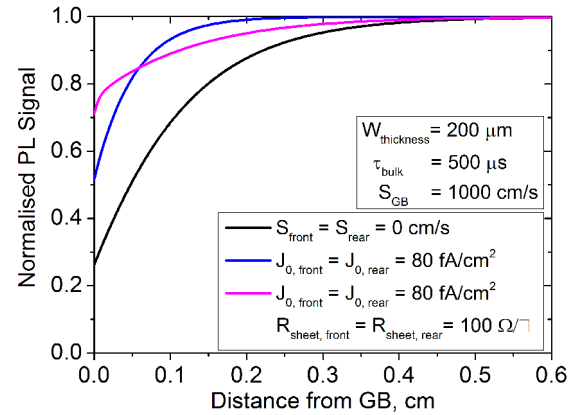


Figure 5: PL profile across a GB with S_{GB} of 1000 cm/s under various surface conditions. Only one side of the PL profile is shown as the PL profile is symmetrical. The bulk lifetimes of the neighboring grains are assumed to be injection independent and are set to be 500 μs . The wafers are illuminated with an incident photon flux of $2.3 \times 10^{17} \text{ cm}^{-2} \text{ s}^{-1}$, at 808 nm.

Moreover, the spatial influence of GBs tends to be larger under open circuit conditions in comparison to short circuit conditions. Under open circuit conditions, carriers can flow freely from the intra-grain regions to the GBs either via the heavily doped regions or bulk diffusion [26, 27]. Under short circuit conditions, most of the carriers that reach pn junction are likely to be collected at metal contacts and extracted to the external circuit instead of flowing into the GBs. This is demonstrated in Fig. 6 which shows a two dimensional simulation, performed with Sentaurus [28], of the electron concentration around a GB with S_{GB} of 1000 cm/s at different operating conditions. In Fig. 6, lateral variation in the electron concentration is due to GB recombination, whereas the vertical variation is caused by charge collection and recombination in the heavily doped regions. It can be seen that the influence of GB is at maximum under open circuit condition. Their impact reduces at maximum power point and is minimal at short circuit conditions in which the carrier density is strongly dominated by charge collection and emitter recombination.

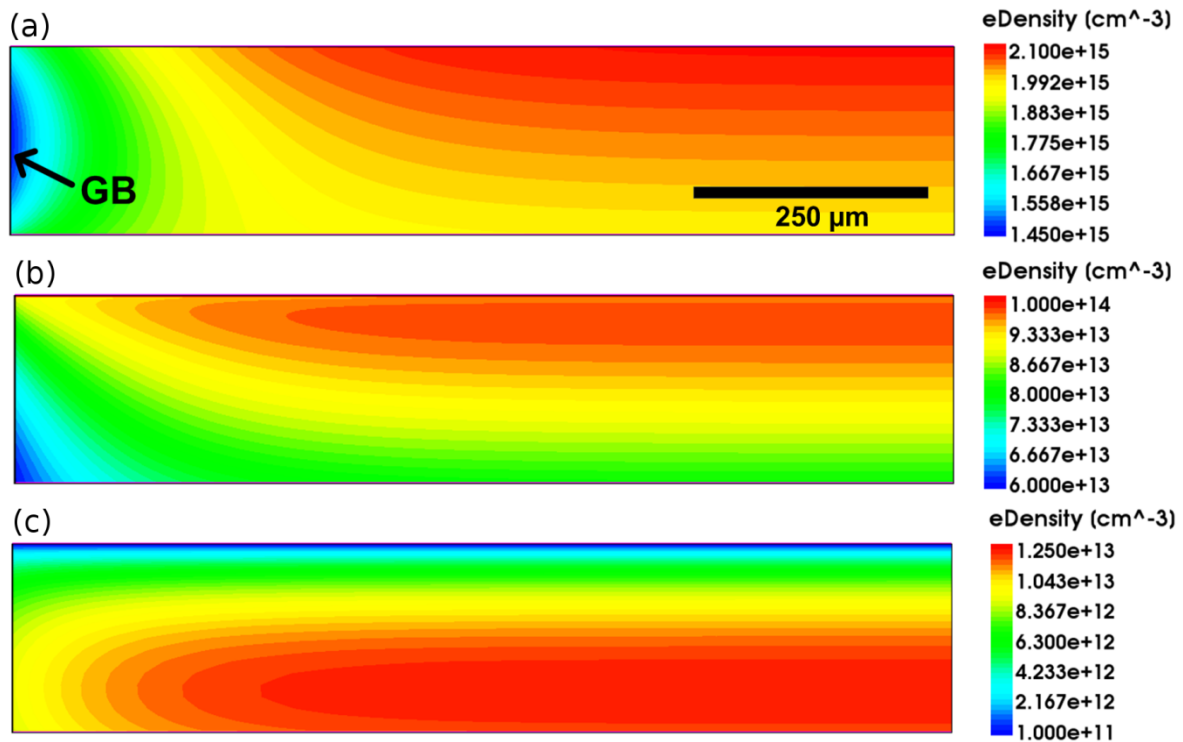


Figure 6: Electron concentration around a GB with S_{eff} of 1000 cm/s at (a) open circuit, (b) maximum power point and (c) short circuit condition. The bulk lifetimes of the neighbouring grains are set to be $500 \mu\text{s}$. The samples are illuminated at approximately one sun. The J_0 for the front and rear surfaces are around 120 fA/cm^2 and 90 fA/cm^2 respectively. The width and thickness of the sample are set to be 1 cm and $200 \mu\text{m}$ respectively. Note the different scale in each figure.

4 CONCLUSIONS

We have performed a direct comparison of the GB behaviour in conventional p-type, n-type and high performance p-type mc-Si materials. It is found that the GBs in the conventional p-type samples are more recombination active than those in the high performance p-type and conventional n-type samples. Hydrogenation is more effective on the n-type samples than p-type samples, being able to deactivate most of the GBs in n-type samples. As-grown GBs in high performance mc-Si are not recombination active and they only become active after gettering or hydrogenation. Annealing experiments reveal that the activation of GBs in the studied high performance mc-Si occurs between 400°C and 550°C and such activation is more likely to be related to the high temperature used in the process, rather than the rapid quenching afterward. Moreover, distinct sub-bandgap PL spectra were detected from GBs that are already active before gettering, and also from gettering-activated GBs, suggesting different origins for their recombination activities.

ACKNOWLEDGMENTS

This work has been supported by the Australian Renewable Energy Agency (ARENA) under project RND009. H. C. Sio acknowledges scholarship support from BT Imaging and the Australian Renewable Energy Agency (ARENA) through the Australian Centre for Advanced Photovoltaics (ACAP). D. M. is supported by an Australian Research Council (ARC) Future Fellowship. H. C. Sio would like to thank A. Y. Liu and

C. Sun for fruitful discussions, as well as E.C. Wang for assistance with sample preparation.

REFERENCES

- [1] J. Chen, T. Sekiguchi, D. Yang, F. Yin, K. Kido, S. Tsunekawa, Electron-beam-induced current study of grain boundaries in multicrystalline silicon, *J. Appl. Phys.*, 96 (2004) 5490-5495.
- [2] T. Buonassisi, A.A. Istratov, M.D. Pickett, M.A. Marcus, T.F. Cizek, E.R. Weber, Metal precipitation at grain boundaries in silicon: Dependence on grain boundary character and dislocation decoration, *Applied Physics Letters*, 89 (2006) 042102.
- [3] A. Stoffers, O. Cojocaru-Mirédin, W. Seifert, S. Zaeferrer, S. Riepe, D. Raabe, Grain boundary segregation in multicrystalline silicon: correlative characterization by EBSD, EBIC, and atom probe tomography, *Progress in Photovoltaics: Research and Applications*, (2015).
- [4] P. Karzel, M. Ackermann, L. Gröner, C. Reimann, M. Zschorsch, S. Meyer, F. Kiessling, S. Riepe, G. Hahn, Dependence of phosphorus gettering and hydrogen passivation efficacy on grain boundary type in multicrystalline silicon, *J. Appl. Phys.*, 114 (2013) 244902.
- [5] I. Takahashi, N. Usami, H. Mizuseki, Y. Kawazoe, G. Stokkan, K. Nakajima, Impact of type of crystal defects in multicrystalline Si on electrical properties and interaction with impurities, *J. Appl. Phys.*, 109 (2011) 033504.
- [6] S. Joonwichien, S. Matsushima, N. Usami, Effects of crystal defects and their interactions with impurities on

- electrical properties of multicrystalline Si, *J. Appl. Phys.*, 113 (2013) 133503.
- [7] H. Nouri, M. Bouaïcha, M. Ben Rabha, B. Bessaïfs, Gettering effect in grain boundaries of multi-crystalline silicon, *physica status solidi (c)*, 9 (2012) 1937-1941.
- [8] L.J. Geerligs, Y. Komatsu, I. Röver, K. Wambach, I. Yamaga, T. Saitoh, Precipitates and hydrogen passivation at crystal defects in n- and p-type multicrystalline silicon, *J. Appl. Phys.*, 102 (2007) 093702.
- [9] T. Jiang, X. Yu, X. Gu, D. Yang, G. Rozgonyi, Hydrogenation of interface states at a clean grain boundary in the direct silicon bonded wafer, *physica status solidi (a)*, 209 (2012) 990-993.
- [10] M.I. Bertoni, S. Hudelson, B.K. Newman, D.P. Fenning, H.F.W. Dekkers, E. Cornagliotti, A. Zuschlag, G. Micard, G. Hahn, G. Coletti, B. Lai, T. Buonassisi, Influence of defect type on hydrogen passivation efficacy in multicrystalline silicon solar cells, *Progress in Photovoltaics: Research and Applications*, 19 (2011) 187-191.
- [11] J. Chen, D. Yang, Z. Xi, T. Sekiguchi, Electron-beam-induced current study of hydrogen passivation on grain boundaries in multicrystalline silicon: Influence of GB character and impurity contamination, *Physica B: Condensed Matter*, 364 (2005) 162-169.
- [12] H.C. Sio, T. Trupke, D. Macdonald, Quantifying carrier recombination at grain boundaries in multicrystalline silicon wafers through photoluminescence imaging, *J. Appl. Phys.*, 116 (2014) 244905.
- [13] H.C. Sio, S.P. Phang, T. Trupke, D. Macdonald, Impact of Phosphorous Gettering and Hydrogenation on the Surface Recombination Velocity of Grain Boundaries in p-Type Multicrystalline Silicon, *Photovoltaics, IEEE Journal of*, 5 (2015) 1357-1365.
- [14] D. Walter, A. Fell, E. Franklin, D. Macdonald, B. Mitchell, T. Trupke, The Impact of Silicon CCD Photon Spread on Quantitative Analyses of Luminescence Images, *Photovoltaics, IEEE Journal of*, 4 (2014) 368-373.
- [15] R.A. Sinton, Predicting multi-crystalline solar cell efficiency from life-time measured during cell fabrication, in: *Photovoltaic Energy Conversion, 2003. Proceedings of 3rd World Conference on*, 2003, pp. 1028-1031 Vol.1022.
- [16] D. Macdonald, L.J. Geerligs, Recombination activity of interstitial iron and other transition metal point defects in p- and n-type crystalline silicon, *Applied Physics Letters*, 85 (2004) 4061-4063.
- [17] C. Sun, F.E. Rougieux, D. Macdonald, A unified approach to modelling the charge state of monatomic hydrogen and other defects in crystalline silicon, *J. Appl. Phys.*, 117 (2015) 045702.
- [18] H.C. Sio, D. Macdonald, Direct comparison of the electrical properties of multicrystalline silicon materials for solar cells: conventional p-type, n-type and high performance p-type, *Accepted to Solar Energy Materials and Solar Cells*, (2015).
- [19] R. Sauer, J. Weber, J. Stolz, E.R. Weber, K.H. Küsters, H. Alexander, Dislocation-related photoluminescence in silicon, *Appl. Phys. A*, 36 (1985) 1-13.
- [20] H.T. Nguyen, F.E. Rougieux, F. Wang, H. Tan, D. Macdonald, Micrometer-Scale Deep-Level Spectral Photoluminescence From Dislocations in Multicrystalline Silicon, *Photovoltaics, IEEE Journal of*, 5 (2015) 799-804.
- [21] M. Tajima, Y. Iwata, F. Okayama, H. Toyota, H. Onodera, T. Sekiguchi, Deep-level photoluminescence due to dislocations and oxygen precipitates in multicrystalline Si, *J. Appl. Phys.*, 111 (2012) 113523.
- [22] T. Buonassisi, A.A. Istratov, M.D. Pickett, M. Heuer, J.P. Kalejs, G. Hahn, M.A. Marcus, B. Lai, Z. Cai, S.M. Heald, T.F. Cizek, R.F. Clark, D.W. Cunningham, A.M. Gabor, R. Jonczyk, S. Narayanan, E. Saunar, E.R. Weber, Chemical natures and distributions of metal impurities in multicrystalline silicon materials, *Progress in Photovoltaics: Research and Applications*, 14 (2006) 513-531.
- [23] T. Buonassisi, M. Heuer, A.A. Istratov, M.D. Pickett, M.A. Marcus, B. Lai, Z. Cai, S.M. Heald, E.R. Weber, Transition metal co-precipitation mechanisms in silicon, *Acta Materialia*, 55 (2007) 6119-6126.
- [24] H.C. Sio, S.P. Phang, Y. Wan, W. Liang, T. Trupke, S. Cao, D. Hu, Y. Wan, D. Macdonald, The influence of crystal orientation on surface passivation in multicrystalline silicon, *Proceeding of the 39th IEEE Photovoltaic Specialists Conference (PVSC)*, Tampa, USA, (2013) 1770-1775.
- [25] H.C. Sio, Z. Xiong, T. Trupke, D. Macdonald, Imaging crystal orientations in multicrystalline silicon wafers via photoluminescence, *Applied Physics Letters*, 101 (2012) 082102.
- [26] P.P. Altermatt, A. Cuevas, G. Heiser, Modelling the impact of inhomogeneous recombination losses on mc-Si cell efficiency, in: *Technical Digest of the 14th International Photovoltaic Science and Engineering Conference*, Bangkok, Thailand, 2004, pp. 243-244.
- [27] B. Michl, M. Rüdiger, J.A. Giesecke, M. Hermle, W. Warta, M.C. Schubert, Efficiency limiting bulk recombination in multicrystalline silicon solar cells, *Solar Energy Materials and Solar Cells*, 98 (2012) 441-447.
- [28] Synopsys, Sentaurus Device User Guide, Version 2013.03, in, 2013.